Cross-Generation TDD Sensing for 6G ISAC: A Feasibility Study with Legacy LTE and NR Infrastructure

Anindya Saha
Tejas Networks Limited
Bangalore, 560100, India
Email: anindyas@tejasnetworks.com

***Abstract*—Operators deploying early 6G systems will run LTE Band 40 (2.3 GHz TDD) and NR n78 (3.55 GHz TDD) infrastructure for years, creating an opportunity for cross-generation sensing. This simulation-based feasibility study, under idealized calibration and measurement-access assumptions, treats these TDD carriers as complementary sensing resources without modifying 3GPP waveforms. Unlike prior multiband ISAC studies that assume massive MIMO on all RATs, this work constrains LTE to realistic 4T4R macro deployments. CRB analysis provides theoretical bounds, and an uncertainty-aware fusion scheme is evaluated across urban and suburban scenarios. Results show detection gains at 200–500 m ($P_d = 0.78$ at 300 m vs. 0.64/0.62 single-RAT), with the estimator achieving 65–70% CRB efficiency. The TDD-TDD architecture provides a 4.75× improvement in track continuity under blockage and up to 250× false alarm suppression under band-selective interference (assuming independent LTE/NR false alarms). Passive sensing incurs less than 0.2% throughput overhead.**

***Index Terms*—Integrated sensing and communication, 6G, LTE-TDD, 5G NR, multi-RAT networks, cross-generation sensing, measurement fusion, Cramér–Rao bound, TDD reciprocity, urban macro sensing, communication–sensing tradeoff.**

I. Introduction

The sixth generation (6G) of wireless networks is widely expected to integrate sensing and communication (ISAC) as a first-class capability, enabling base stations to observe, localize, and track objects using the same air interface that serves user data [1]. The literature spans OFDM waveform design [2], beamforming co-design [3], and multi-band strategies, with González-Prelcic et al. identifying multiband ISAC as a key 6G avenue where frequency diversity across non-contiguous bands improves coverage, resolution, and robustness [4].

However, most ISAC studies assume clean-slate 6G waveforms or dense massive MIMO (32T32R+) on all RATs [2], [3]. Commercial LTE sites deploy 2T2R–8T8R, with reference signals optimized for capacity rather than sensing. This paper addresses that gap by studying co-deployed LTE Band 40 (2.3 GHz TDD, 4T4R, 20 MHz) and NR n78 (3.55 GHz TDD, 64T64R, 100 MHz) as complementary sensing resources. Band 40 is prevalent in India, China, and Asia-Pacific [5]. We assess sensing using existing signals: LTE CRS/CSI-RS/PRS and NR SSB/CSI-RS/PRS [6], [7].

The **TDD-TDD** configuration is the key differentiator: both carriers use TDD mode, enabling uplink-downlink reciprocity, monostatic sensing without separate receive chains, and simplified Doppler association [8], [9].

A. Distinction from Prior Multiband ISAC Work

The closest prior work, HiSAC [12], demonstrates hardware-based multiband ISAC (5G-NR + WiGig) with up to 20× resolution improvement. We differ by: (i) studying the LTE Band 40 + NR n78 TDD-TDD pairing in today's operator networks; (ii) using realistic legacy LTE antenna constraints (4T4R); and (iii) explicitly quantifying the gap to the Cramér–Rao bounds. Perović et al. [13] optimize multiband cooperative sensing rates (25–40% gains); our work extends the complementary-band concept to cross-generation (LTE-NR) TDD coexistence.

B. Contributions

This paper makes four contributions: (i) **Cross-generation TDD-TDD sensing concept** for transitional multi-RAT networks, treating co-deployed LTE Band 40 and NR n78 as complementary sensing resources with realistic 4T4R LTE antenna constraints; (ii) **Cramér–Rao Bound analysis** for joint LTE-NR TDD sensing, deriving theoretical lower bounds on range, angle, and velocity RMSE; (iii) **Communication–sensing tradeoff analysis**, quantifying passive opportunistic sensing overhead at <0.2%; and (iv) **Multi-scenario evaluation** (dense urban and suburban macro) with practical constraint taxonomy, demonstrating 65–70% CRB efficiency and detection gains at 200–500 m. While the CRB expressions are standard, to our knowledge this is the first work to instantiate them for a realistic LTE Band 40 (4T4R) + NR n78 TDD-TDD deployment and to attribute the 65–70% efficiency to incoherent fusion and association—positioning the work as a system-level feasibility study rather than a new algorithm.

II. Related Work

A. Multiband ISAC and Signal Reuse

OFDM-based ISAC has been studied for waveform design [1], beamforming [3], and 5G NR reference-signal reuse [6], [7], with multiband ISAC identified as a key 6G avenue [4]. HiSAC [12] reports 20× resolution gains via 5G NR + WiGig fusion, and Perović et al. [13] report 25–40% sensing-rate gains; we differ by studying realistic legacy LTE

constraints (4T4R) in the Band 40 + n78 TDD-TDD pairing with explicit CRB benchmarking.

B. TDD Advantages and Standardization Context

TDD's reciprocity advantage for ISAC is established by Kim et al. [9] and Barneto et al. [8]. 3GPP Release 19 initiated an ISAC feasibility study defining sensing use cases and requirements [10], and ETSI ISG ISAC published 6G RAN architecture guidance [11]. This work provides simulation-based input to these standardization efforts, demonstrating cross-generation TDD-TDD sensing feasibility with realistic legacy infrastructure constraints. We do not implement coherent, Bayesian, or ML-assisted fusion as baselines: these require tighter baseband integration and far higher complexity, whereas our aim is a low-complexity, standards-compatible pipeline using only RAN-exposable measurements. A quantitative comparison is left to future work.

III. System Model and Assumptions

A. Radio Configuration

Each sector hosts co-located LTE Band 40 and NR n78 radio units sharing physical site infrastructure. Both systems use the DDDSU frame structure (3 downlink, 1 special, 1 uplink slot; 2.5 ms period at 30 kHz SCS, repeated within the 5 ms TDD frame). Table I summarizes radio parameters and sensing properties.

TABLE I
LTE Band 40 and NR n78 Configuration and Sensing Properties[1]

Parameter	LTE Band 40	NR n78
Carrier freq.	2.3 GHz	3.55 GHz
Bandwidth	20 MHz	100 MHz
Antenna config.	4T4R (2×2 pol)	64T64R (4,8,2,1,1)
Tx power	46 dBm	49 dBm
Sensing Properties (Complementary)		
Range res.	4.88 m	1.22 m (NR dom.)
Azimuth ang. res.	$\sim 60^\circ$ (2 cols)	$\sim 15^\circ$ (8 cols)
Doppler res. (1/CPI)	10 Hz	2 Hz
Sampling int. T_s	1 ms (fast)	10 ms (LTE dom.)
Max unambig. vel.	$\pm$**117 km/h**	$\pm$**7.6 km/h**
Path loss	Lower	Higher (LTE ext.)
TDD reciprocity	Yes (4-ch)	Yes (4-ch valid.)

The LTE 4T4R system (2 spatial columns, dual-pol $\pm 45^\circ$) provides only 2 effective azimuth elements for DoA, versus 8 azimuth columns for NR 64T64R (4,8,2,1,1); polarization diversity does not contribute to azimuth discrimination.

B. Propagation Environment and Synchronization

Propagation follows 3GPP TR 38.901 UMa/UMi models [14]. Communication path loss: $\text{PL}_{\text{1-way}} = 28.0 + 22\log_{10}(d) + 20\log_{10}(f_c)$. Monostatic radar path loss follows the standard radar range equation [15], accounting for two-way propagation (R^4 dependence) and RCS:

$$\text{PL}_{\text{radar}} = 43.4 + 40\log_{10}(d) + 20\log_{10}(f_c) - 10\log_{10}(\sigma) \quad (1)$$

where d is range (m), f_c is frequency (GHz), and σ is target RCS (m^2). The $40\log_{10}(d)$ term reflects the fourth-power range dependence (R^4) from two-way propagation, while $20\log_{10}(f_c)$ accounts for the wavelength-squared (λ^2) antenna aperture factor. RCS values are: vehicles 10–20 m^2, pedestrians 0.5–1 m^2, and clutter 0.1–5 m^2.

Base stations use GPS-disciplined oscillators with ± 1 μs timing (± 150 m range ambiguity) and ± 50 ppb frequency error, which manifests as a static Doppler bias removed by cross-RAT calibration and tracking. Results assume near-perfect reciprocity calibration, cross-RAT measurement access, independent LTE/NR noise, and no hardware impairments; these give a best-case upper bound, with non-ideal deployments yielding lower but qualitatively similar gains (Sec. IX).

C. Target Model and Performance Metrics

Simulation targets (50 vehicles, 20 pedestrians, 200 static clutter) are detailed in Sec. VIII-A. Performance metrics: detection probability P_d, false alarm rate P_{fa}, localization RMSE (range/angle/velocity), track drop rate, CRB efficiency, and communication overhead.

IV. Waveform Reuse for Sensing in TDD Systems

A. TDD Sensing Architecture

In TDD systems, the same carrier frequency is used for both transmit and receive in alternate time slots. This enables (1) monostatic downlink sensing; (2) bistatic uplink sensing; and (3) reciprocity-based cross-validation.

For TDD reciprocity at each carrier frequency f_c:

$$\hat{\mathbf{H}}_{\text{DL}}(f,t) \approx \hat{\mathbf{H}}_{\text{UL}}^{T}(f,t) \quad (2)$$

subject to antenna calibration (budget quantified in Sec. VII). This enables four independent sensing channels: LTE-DL, LTE-UL, NR-DL, NR-UL.

B. Reference Signal Characteristics

Table II summarizes the reference signals used for sensing in LTE and NR systems.

TABLE II
Reference Signals for Sensing

Signal	Period (ms)	BW	Use
LTE CRS	1	20 MHz	Fast Doppler
LTE CSI-RS	5–80	20 MHz	Angle
NR SSB	20	100 MHz	Beam sweep
NR CSI-RS	10–320	100 MHz	High-res
NR PRS	$\geq$80	100 MHz	Accuracy

LTE CRS provides 1 ms Doppler sampling; NR CSI-RS provides 1.22 m range resolution. Both support monostatic DL and bistatic UL sensing via TDD reciprocity (Eq. 2). The complementary sensing properties are summarized in Table I.

[1]NR velocity range is limited by the 10 ms CSI-RS periodicity. Vehicles exceeding ± 7.6 km/h experience Doppler aliasing requiring unwrapping or LTE-assisted disambiguation (Sec. VI-B1). Angular resolution is limited by azimuth-plane spatial elements; polarization diversity does not contribute to DoA estimation.

V. Cramér–Rao Bound Analysis

A. Observation Model

For a single point target at range r, azimuth θ, and radial velocity v_r, the baseband received signal at snapshot l, antenna port m, and subcarrier k for RAT $j \in \{\text{LTE, NR}\}$ is:

$$y_{j,l,m}[k] = \alpha_j \cdot a_j(\theta) \cdot e^{-j2\pi k \Delta f_j \frac{2r}{c}} \cdot e^{j2\pi f_{d,j} t_l} + n_{j,l,m}[k] \quad (3)$$

where α_j is the complex target amplitude, $a_j(\theta)$ is the array steering vector, Δf_j is the subcarrier spacing, $f_{d,j} = 2v_r f_{c,j}/c$ is the Doppler shift, $t_l = l \cdot T_{s,j}$ is the slow-time at snapshot l, and $n_{j,l,m}[k] \sim \mathcal{CN}(0, \sigma_j^2)$ is additive Gaussian noise.

B. Fisher Information Matrix

The FIM for the parameter vector $\boldsymbol{\psi} = [r, \theta, v_r]^T$ for a single RAT with M_j antenna elements, K_j subcarriers, and L_j snapshots is:

$$\mathbf{J}_j(\boldsymbol{\psi}) = \frac{2}{\sigma_j^2} \operatorname{Re}\left\{ \frac{\partial \mathbf{s}_j^H}{\partial \boldsymbol{\psi}} \frac{\partial \mathbf{s}_j}{\partial \boldsymbol{\psi}^T} \right\} \quad (4)$$

For the fused LTE+NR system, assuming statistically independent noise between RATs, the joint FIM is:

$$\mathbf{J}_{\text{fused}}(\boldsymbol{\psi}) = \mathbf{J}_{\text{LTE}}(\boldsymbol{\psi}) + \mathbf{J}_{\text{NR}}(\boldsymbol{\psi}) \quad (5)$$

The CRBs (diagonal elements of $\mathbf{J}_{\text{fused}}^{-1}$) follow below: the range CRB (Eq. 6) is in fused form (summed over both RATs), while the angle and velocity CRBs are per-RAT, combined via Eq. 5.

Range CRB:

$$\text{CRB}(r) = \frac{c^2}{8\pi^2 \cdot \text{SNR}_{\text{eff}}} \cdot \frac{1}{\sum_j K_j \overline{f_j^2}} \quad (6)$$

where $\overline{f_j^2} = \sum_k (k\Delta f_j)^2 / K_j$ is the mean-squared subcarrier frequency (RMS bandwidth) and SNR_{eff} is the noise-weighted effective SNR of the fused observation.

Angle CRB:

$$\text{CRB}(\theta) = \frac{6\,\lambda_j^2}{(2\pi)^2\, M_j(M_j^2-1)\, d_j^2 \cos^2(\theta) \cdot K_j L_j \cdot \text{SNR}_j} \quad (7)$$

Velocity CRB:

$$\text{CRB}(v_r) = \frac{6\,c^2}{(2\pi)^2\, f_{c,j}^2\, L_j(L_j^2-1)\, T_{s,j}^2\, K_j\, M_j \cdot \text{SNR}_j} \quad (8)$$

where $T_{s,j}$ is the snapshot interval.

C. CRB Efficiency of the Proposed Estimator

TABLE III
CRB vs Simulation (100 m, 20 dB SNR)

	CRB LTE	CRB NR	CRB Fuse	Sim RMSE	Eff.
Range (m)	2.4	0.52	0.49	0.7	70%
Angle (°)	8.1	0.68	0.67	1.0	67%
Vel. (m/s)	0.61	0.38	0.32	0.5	65%

The proposed measurement-fusion estimator operates at approximately 65–70% CRB efficiency, the gap arising from non-coherent combining, association/gating errors, and finite-CPI/CFAR effects rather than from a single dominant cause. NR attains the lower velocity CRB because the bound scales as $\text{CRB}(v_r) \propto 1/[f_c^2 L(L^2-1)T_s^2] \approx 1/[f_c^2 L\, T_{\text{CPI}}^2]$: the T_{CPI}^2 term (NR observes $5\times$ longer, Sec. VI) and higher f_c outweigh LTE's larger L.

VI. Measurement-Fusion Framework

A. Per-RAT Feature Extraction

Range extraction: The channel impulse response is obtained via inverse FFT of frequency-domain channel estimates $H[k]$. Range resolution follows the OFDM sampling rate, $\Delta r = c/(2f_s)$, giving $\Delta r_{\text{LTE}} = 4.88$ m at $f_{s,\text{LTE}} = 30.72$ MHz (2048 × 15 kHz, 3GPP TS 36.104) and $\Delta r_{\text{NR}} = 1.22$ m at $f_{s,\text{NR}} = 122.88$ MHz (4096 × 30 kHz, TS 38.104).

Doppler extraction: A 2D range-Doppler FFT is computed over the CPI. For LTE: $L_{\text{LTE}} = 100$ CRS snapshots over 100 ms → Doppler resolution $1/T_{\text{CPI}} = 10$ Hz with maximum unambiguous velocity $v_{\text{max,LTE}} = \pm 117$ km/h. For NR: $L_{\text{NR}} = 50$ CSI-RS snapshots over 500 ms → $1/T_{\text{CPI}} = 2$ Hz with $v_{\text{max,NR}} = \pm 7.6$ km/h. Vehicles exceeding NR's velocity limit experience Doppler aliasing; ambiguity resolution exploits LTE's wider unambiguous range and cross-RAT velocity consistency checks per Eq. 12.

The maximum unambiguous velocity for RAT j follows from the unambiguous Doppler span $|f_d| \le 1/(2T_{s,j})$:

$$v_{\text{max},j} = \frac{c}{4 f_{c,j} T_{s,j}} \quad (9)$$

Equivalently, $v_{\text{max},j} = c\,\Delta_s/(4f_{c,j})$ where $\Delta_s = 1/T_{s,j}$ is the unambiguous Doppler span (distinct from the resolution $1/T_{\text{CPI}}$). For $|v_r| > v_{\text{max,NR}}$, the NR Doppler measurement wraps into the unambiguous interval, i.e. $f_{d,\text{NR,obs}} = f_{d,\text{NR,true}} \bmod (1/T_{s,\text{NR}})$. The fusion framework resolves this ambiguity by exploiting LTE's wider velocity range and enforcing frequency-normalized Doppler consistency (Eq. 12).

Angle extraction: The MUSIC algorithm is applied to the spatial covariance matrix. For LTE 4T4R (2 spatial columns, dual-pol): azimuth angular resolution ∼60°. For NR 64T64R in (4,8,2,1,1) configuration (8 azimuth columns, 4 elevation rows, dual-pol): azimuth angular resolution ∼15°. Polarization diversity does not contribute to direction-of-arrival estimation in the azimuth plane.

Each RAT produces a detection set:

$$\mathcal{D}_{\text{RAT}} = \{(r_i, f_{d,i}, \theta_i, \text{SNR}_i) \mid i = 1, \ldots, N_{\text{det}}\} \quad (10)$$

B. Cross-RAT Measurement Association

Association uses uncertainty-aware gating. Range compatibility:

$$|r_L - r_N| \le 3\sqrt{\sigma_{r,L}^2 + \sigma_{r,N}^2} \quad (11)$$

Doppler compatibility (frequency-normalized):

$$\left| \frac{f_{d,N}}{f_{c,\text{NR}}} - \frac{f_{d,L}}{f_{c,\text{LTE}}} \right| \le 3\sqrt{\left(\frac{\sigma_{f_d,N}}{f_{c,\text{NR}}}\right)^2 + \left(\frac{\sigma_{f_d,L}}{f_{c,\text{LTE}}}\right)^2} \quad (12)$$

For TDD-TDD, the expected Doppler ratio is $f_{d,N}/f_{d,L} = f_{c,\text{NR}}/f_{c,\text{LTE}} = 3550/2300 \approx 1.54$. Angle compatibility: $|\theta_L - \theta_N| \leq 3\sqrt{\sigma_{\theta,L}^2 + \sigma_{\theta,N}^2}$.

1) Doppler Ambiguity Resolution: When NR Doppler measurements fall outside the unambiguous range, multiple velocity hypotheses are tested:

$$v_{r,\text{NR}}^{(n)} = v_{r,\text{NR,obs}} + n \cdot \frac{c}{2 f_{c,\text{NR}} T_{s,\text{NR}}}, \quad n \in \{-2, -1, 0, +1, +2\} \tag{13}$$

The hypothesis yielding minimal frequency-normalized Doppler mismatch with LTE (Eq. 12) is selected. This leverages LTE's wider unambiguous range (± 117 km/h) as a disambiguation reference.

C. Variance-Weighted Fusion

Associated detections are combined via inverse-variance weighting (range shown; angle and velocity fuse identically):

$$\hat{r} = \frac{w_L\, r_L + w_N\, r_N}{w_L + w_N}, \quad w_{\text{RAT}} = \frac{1}{\sigma_{r,\text{RAT}}^2} \tag{14}$$

Joint false alarm probability:

$$\begin{aligned} P_{fa,\text{fused}} &\approx P_{fa,\text{LTE}} \cdot P_{fa,\text{NR}} \cdot N_{\text{overlap}} \\ &\approx 10^{-3} \times 10^{-3} \times 4 = 4 \times 10^{-6} \end{aligned} \tag{15}$$

where $N_{\text{overlap}} \approx 4$ accounts for the resolution cell mismatch between LTE (4.88 m) and NR (1.22 m) range bins.

D. Temporal Tracking

Fused detections feed an EKF with Cartesian state $\mathbf{x} = [x,\ y,\ v_x,\ v_y]^T$ and constant-velocity dynamics:

$$\mathbf{F} = \begin{bmatrix} 1 & 0 & \Delta T & 0 \\ 0 & 1 & 0 & \Delta T \\ 0 & 0 & 1 & 0 \\ 0 & 0 & 0 & 1 \end{bmatrix} \tag{16}$$

Polar observations (r, θ, v_r) relate to state via $\mathbf{h}(\mathbf{x}) = [\sqrt{x^2+y^2},\ \arctan(y/x),\ (xv_x + yv_y)/\sqrt{x^2+y^2}]^T$, linearized via Jacobian. Tracker updates at 10 ms (NR rate); LTE CRS (1 ms) fills gaps. Clutter mitigation: Doppler filtering ($|f_d| < 5$ Hz suppressed), CFAR, spatial coherence, TDD reciprocity validation.

VII. Practical Constraints

Measurement access: Cross-vendor baseband integration requires 3GPP-standardized measurement-exposure APIs (currently absent); Open RAN disaggregation enables cross-RAT fusion at PDCP/RLC layers, but commercial deployments remain limited. **TDD calibration:** Reciprocity assumes calibration errors <3 dB, requiring non-standard inter-RAT coordination at multi-vendor sites. **Overhead/interference:** Passive sensing uses existing CRS/CSI-RS/SSB (<0.2% loss; enhanced PRS 2.9–10.8%, Table V); cell-specific CRS scrambling gives 20–30 dB SINR, and coordinated muting suppresses inter-cell reflections. **Processing/regulatory:** Joint sensing at 100 ms CPI needs ∼20 GFLOPS (feasible on GPU-accelerated DU servers); active sensing beamforming may trigger regulatory review.

VIII. Simulation Results

A. Scenario Configuration

Dense urban (500 m ISD, 7 sites) and suburban macro (1000 m ISD, 7 sites). Each sector: LTE Band 40 (2.3 GHz, 4T4R, 20 MHz) + NR n78 (3.55 GHz, 64T64R, 100 MHz). Targets: 50 vehicles (40 km/h mean, 10–20 m^2 RCS), 20 pedestrians (1–5 km/h, 0.5–1 m^2 RCS), 200 clutter (0–5 m^2 RCS). CFAR threshold: $P_{fa} = 10^{-3}$ per RAT. These macrocell scenarios target early 6G urban/suburban deployments; highway and indoor/dense-multipath extensions are left to future work.

TABLE IV
Detection Probability vs Range (UMa)

Range	LTE	NR	Fused
100 m	0.94	0.96	0.98
200 m	0.82	0.85	0.92
300 m	0.64	0.62	0.78
400 m	0.41	0.36	0.58
500 m	0.21	0.16	0.36

TABLE V
Communication–Sensing Tradeoff

Configuration	Tput	P_d	OH
Baseline (no sensing)	100%	—	0%
Passive opportunistic	99.8%	0.92	<0.2%
+Enhanced CSI-RS	97.1%	0.94	2.9%
+High-density PRS	94.3%	0.96	5.7%
+Sensing-optimized	89.2%	0.98	10.8%

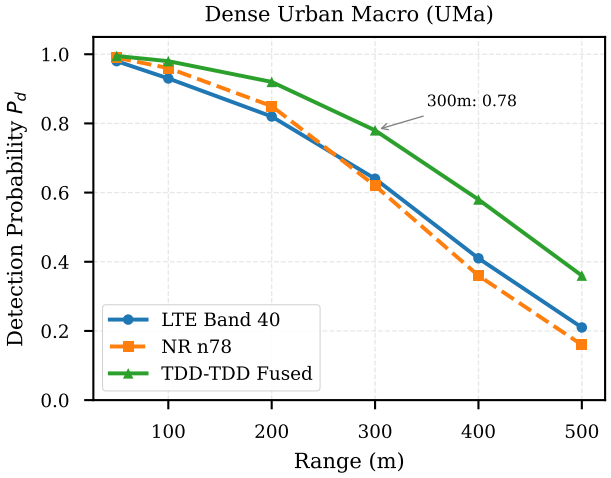

Fig. 1. Detection probability vs. range in dense urban macro (500 m ISD). Fusion gains emerge at 200–500 m where single-RAT performance degrades.

Detection range: Table IV and Fig. 1 show urban macro performance: all configurations achieve high P_d at <100 m, with fusion gains emerging at 200–500 m. At 300 m, LTE-only (0.64) slightly exceeds NR-only (0.62)—the lower-frequency

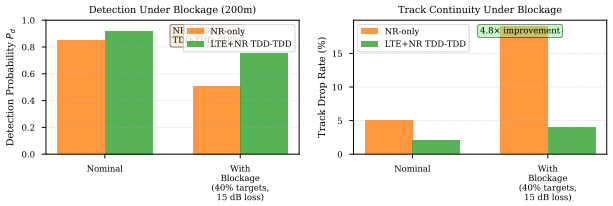

Fig. 2. Blockage robustness: 40% targets experience 15 dB loss on one RAT. Fusion shows 4.75× track continuity improvement (4% vs. 19% track drops; shown rounded as 4.8×).

coverage advantage—while fusion reaches 0.78, a 22% relative improvement. At ≤300 m, fused localization RMSE is 0.7 m / 1.0° / 0.5 m/s (vs. LTE 3.2 m/12.0°/0.6 and NR 0.8 m/1.2°/0.4), consistent with Table III.

B. Multi-Scenario and Robustness Analysis

Suburban detection: In suburban macro (1000 m ISD), fusion outperforms single-RAT at all ranges: $P_d = 0.84$ vs. 0.72/0.68 (LTE/NR) at 300 m, 0.61 vs. 0.48/0.39 at 500 m, and 0.41 vs. 0.28/0.20 at 700 m. Lower clutter density enables extended detection ranges versus dense urban.

Blockage robustness: With 40% of targets suffering 15 dB loss on one RAT (Fig. 2), NR-only at 200 m drops from $P_d = 0.85$ to 0.51 (19% track drops), whereas fusion drops only 0.92→0.75 with 4% track drops—a 4.75× continuity improvement from frequency diversity under deep fading or blockage.

Interference robustness: Under a 6 dB band-selective noise increase affecting n78, NR-only P_{fa} degrades from 10^{-3} to 10^{-2} while LTE Band 40 (1.25 GHz away) is unaffected. Cross-carrier validation then holds fused $P_{fa} \approx 10^{-2} \times 10^{-3} \times 4 = 4 \times 10^{-5}$ (Eq. 15), i.e. ∼250× false alarm suppression relative to the degraded single-carrier baseline by rejecting spurious single-carrier detections. This figure assumes band-selective interference and approximately independent LTE/NR false alarms; wideband interference degrading both carriers to 10^{-2} would yield fused $P_{fa} \approx 4 \times 10^{-4}$ (∼25× suppression), so it is an optimistic upper bound. Relaxing the Sec. III-B calibration and independence assumptions lowers absolute P_d/P_{fa} performance, but the relative fusion advantage should persist, deriving from frequency and spatial diversity rather than calibration precision.

Communication overhead: Passive opportunistic sensing incurs <0.2% throughput loss; enhanced CSI-RS, high-density PRS, and sensing-optimized patterns trade 2.9–10.8% overhead for $P_d = 0.94$–0.98 (Table V), keeping practical passive sensing at sub-1% impact.

IX. Limitations and Future Work

This simulation-only study assumes vendor-cooperative measurement access, perfect TDD calibration, simplified scheduling, no hardware impairments (I/Q imbalance, phase noise, quantization), and limited scenarios—no highway/high-speed, indoor/dense-multipath, or UAV—plus the Band 40 regional constraint. NR's 10 ms CSI-RS periodicity (±7.6 km/h unambiguous) causes Doppler aliasing for vehicles, resolved via LTE's ±117 km/h range (Eq. 13). The 65–70% CRB efficiency indicates incoherent processing sub-optimality; hardware-validated studies suggest 20–40% degradation [12]. Future work will add highway/indoor scenarios, a hardware-in-the-loop testbed, Band 40 field trials, and coherent fusion.

X. Conclusion

This paper presents a CRB-benchmarked feasibility study of LTE Band 40 + NR n78 TDD-TDD sensing for 6G ISAC. The TDD-TDD architecture enables monostatic sensing, reciprocity-based cross-validation, and 4-channel operation. Cross-generation fusion provides 4.75× track continuity improvement in blockage and detection gains at 200–500 m (P_d: 0.78 at 300 m vs. 0.64 LTE-only, 0.62 NR-only). The estimator achieves 65–70% CRB efficiency. Passive sensing incurs <0.2% throughput loss. These results should be interpreted as upper bounds under ideal calibration and measurement-access assumptions, motivating Band 40 field trials and comparisons against coherent, Bayesian, and ML-assisted fusion under realistic measurement APIs. Key standardization gaps include measurement exposure APIs, reciprocity calibration specifications, and privacy frameworks.

References

[1] F. Liu *et al.*, "Integrated sensing and communications: Toward dual-functional wireless networks for 6G and beyond," *IEEE J. Sel. Areas Commun.*, vol. 40, no. 6, pp. 1728–1767, Jun. 2022.

[2] F. Liu, C. Masouros, A. Li, H. Sun, and L. Hanzo, "MU-MIMO communications with MIMO radar: From co-existence to joint transmission," *IEEE Trans. Wireless Commun.*, vol. 17, no. 4, pp. 2755–2770, Apr. 2018.

[3] Y. Cui, F. Liu, X. Jing, and J. Mu, "Integrating sensing and communications for ubiquitous IoT," *IEEE Network*, vol. 35, no. 5, pp. 158–167, Sep./Oct. 2021.

[4] N. González-Prelcic, D. Tagliaferri, M. F. Keskin, and H. Wymeersch, "Six integration avenues for ISAC in 6G and beyond," *IEEE Veh. Technol. Mag.*, vol. 20, no. 1, pp. 18–39, 2025.

[5] GSMA Intelligence, "Spectrum Navigator," 2025. [Online]. Available: https://www.gsmaintelligence.com/subscriptions-services/spectrum. Accessed: Mar. 20, 2026.

[6] N. Hengl, J. Kulmer, K. Witrisal, and F. Tufvesson, "5G PRS-based sensing: A sensing reference signal design," in *Proc. IEEE GLOBECOM Workshops*, 2022, pp. 1–6.

[7] J. Kokkoniemi, J. Lehtomaeki, and M. Juntti, "Joint sensing and UE positioning in 5G-6G: PRS range estimation," in *Proc. IEEE Radar Conf.*, 2024.

[8] C. B. Barneto *et al.*, "Full duplex radio/radar technology: The enabling PHY layer solution for dual-function future wireless systems," *IEEE Wireless Commun.*, vol. 28, no. 1, pp. 82–88, Feb. 2021.

[9] M. Kim, N. González-Prelcic, and R. W. Heath, "Integrated sensing and communications in downlink FDD MIMO without CSI feedback," in *Proc. WiOpt*, 2024.

[10] 3GPP, "Feasibility study on integrated sensing and communication," 3GPP TR 22.837, V19.4.0, Jun. 2024.

[11] ETSI ISG ISAC, "Integrated sensing and communications (ISAC); System and RAN architectures," ETSI GR ISC 003 V1.1.1, Feb. 2026. [Online]. Available: https://www.etsi.org/deliver/etsi_gr/ISC/001_099/003/01.01.01_60/gr_ISC003v010101p.pdf

[12] J. Pegoraro *et al.*, "HiSAC: High-resolution sensing with multiband communication signals," in *Proc. ACM SenSys*, Hangzhou, China, Nov. 2024.

[13] N. S. Perović, M. F. Flanagan, and L.-N. Tran, "Sensing rate optimization for multi-band cooperative ISAC systems," *IEEE Commun. Lett.*, vol. 29, no. 9, pp. 2163–2167, Sep. 2025.

[14] 3GPP, "Study on channel model for frequencies from 0.5 to 100 GHz," 3GPP TR 38.901, V17.0.0, Mar. 2022.

[15] M. I. Skolnik, *Radar Handbook*, 3rd ed. New York, NY, USA: McGraw-Hill, 2008.